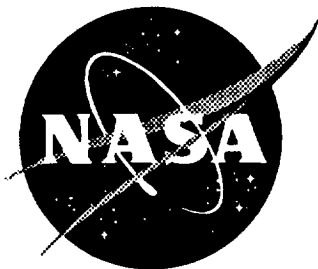# NASA CONTRACTOR REPORT 191523

33p

CRACK-TIP-OPENING ANGLE MEASUREMENTS AND CRACK TUNNELING UNDER STABLE TEARING IN THIN SHEET 2024-T3 ALUMINUM ALLOY

D. S. DAWICKE
Analytical Services and Materials, Inc.
Hampton, VA
        and
M. A. SUTTON
University of South Carolina
Columbia, SC

SEPTEMBER 1993

**National Aeronautics and
Space Administration**

LANGLEY RESEARCH CENTER
Hampton, Virginia 23681-0001

CRACK-TIP-OPENING ANGLE MEASUREMENTS AND CRACK TUNNELING UNDER STABLE TEARING IN THIN SHEET 2024-T3 ALUMINUM ALLOY

D.S. Dawicke[1] and M.A. Sutton[2]

ABSTRACT

The stable tearing behavior of thin sheets of 2024-T3 aluminum alloy was experimentally investigated for middle crack tension specimens having initial flaws that were: (a) flat fatigue cracks (low fatigue stress) and (b) 45° through-thickness slant cracks (high fatigue stress). The critical CTOA values during stable tearing were measured by two independent methods, optical microscopy and digital image correlation. Results from the two methods agreed well.

The CTOA measurements and observations of the fracture surfaces have shown that the initial stable tearing behavior of low and high fatigue stress tests is significantly different. The cracks in the low fatigue stress tests underwent a transition from flat-to-slant crack growth, during which the CTOA values were high and significant crack tunneling occurred. After crack growth equal to about the thickness ($\Delta a > B$), CTOA reached a constant value of 6° and after crack growth equal to about twice the thickness ($\Delta a > 2B$), crack tunneling stabilized. The cracks in the high fatigue stress tests reach the same constant CTOA value after crack growth equal to about the thickness, but produced only a slightly higher CTOA values during initial crack growth. The amount of tunneling in the high fatigue stress tests was about the same as that in the low fatigue stress tests after the flat-to-slant transition.

This study indicates that stress history has an influence on the initial portion of the stable tearing behavior. The initial high CTOA values, in the low fatigue crack tests, coincided with large three-dimensional crack front shape changes due to a variation in the through-thickness crack tip constraint. The measured CTOA reached a constant value of 6° for crack growth of about the specimen thickness. This coincided with the onset of 45° slant crack growth and a stabilized, slightly tunneled (about 20% of the thickness) crack front shape. For crack growth on the 45° slant, the crack front and local field variables are still highly three-dimensional. However, the constant CTOA values and stable crack front shape may allow the process to be approximated with two-dimensional models.

INTRODUCTION

Aging of the commercial transport aircraft fleet has increased concern of fatigue damage developing in pressurized fuselage structures. Prediction of residual strength for a cracked aircraft fuselage structure requires a fracture criterion that can be incorporated into a detailed numerical stress analysis. The fracture criterion should account for both large scale yielding and large amounts of stable crack growth in thin-sheet materials.

---

[1] Senior Scientist, Analytical Services and Materials, Inc., Hampton, VA 23666
[2] Professor, University of South Carolina, Columbia, SC 29208

Numerous fracture mechanics parameters have been proposed to characterize stable crack growth under small scale yielding conditions: average crack opening angle (COA) [1], crack tip opening angle (CTOA) [2,3], crack tip opening displacement (CTOD) [4-6], energy release rate [7], crack tip strain [8], and the J-integral [9]. Landes and Begley [10] used the presence of a substantial HRR zone [11,12] around a crack in a strain hardening material, to justify using the J-integral for small crack growth increments in large-scale yielding conditions. Finite element simulations by Dean and Shih et al. [13-15], theoretical work by Hutchinson and Paris [16], and additional computational analyses by McMeeking and Parks [17] indicate that the crack-tip deformation fields have the HRR singularity for strain hardening materials for "small" amounts of crack growth.

Kobayashi and his coworkers [18-24] have experimentally shown that the surface displacement (u) and the normal strains (ε_{xx}) parallel to the crack line, for a variety of nominally plane stress test specimens, do not have the HRR trends. However, for "small" increments of crack growth, the J-Δa data appear to be reasonably independent of specimen geometry. For larger crack growth increments, the geometry independence of the J-Δa data decreases. Based on scanning electron microscope (SEM) observations, Davidson et al. [25] have suggested that the effective strain very close to the crack tip may be best fitted by a ln(r) form and not the power law form common to the HRR solution. These findings, and others, have prompted the search for other crack growth criteria for large crack growth increments under large-scale plasticity.

Wells [4-6] proposed CTOD as a crack growth criterion for elastic perfectly plastic materials experiencing large increments of crack growth under large-scale plasticity. Since the limiting value for CTOD at the crack tip is zero, an extension of the CTOD-criterion was then proposed by Rice [26] for a stationary crack; the crack tip opening displacement (δ_{45}) was defined to be the opening distance where 45° lines from the crack tip intercept the crack faces. Shih [27,28] suggested that CTOD be defined at the original crack tip location throughout crack growth. Hellman and Schwalbe [29-30] have used this idea to develop δ_5-Δa resistance curves, where the δ_5 parameter is the CTOD measured at the original fatigue crack tip location.

2

Anderson [2] and de Koning [3] suggested that the slope of the crack tip opening profile, CTOA, be used as a parameter characterizing the fracture process. The CTOA criterion assumes that a crack will stably tear when the angle made by the crack faces reaches a critical value. Kanninen [31-33] defined CTOA as the ratio of the crack tip opening displacement to a fixed distance behind the current crack tip location. More recently, Demofonti and Rizzi [34] and Newman et al. [35] have obtained experimental data that indicates that CTOA decreases to a constant value after a small amount of crack growth (about equal to the sheet thickness). Computational studies of stable crack growth were performed by Newman et al. [36, 37] and Brock and Yuan [38] to assess the viability of a CTOA-based fracture criterion for numerical simulations. Both investigators determined that the use of a critical CTOA value in numerical modeling of crack growth was viable. In particular, Brock and Yuan found that CTOA - Δa curves were little affected by specimen geometry. For fully plastic crack growth, CTOA was found to reach a "stable" phase when plasticity extended throughout the uncracked ligament. The stable phase was preceded by a large decrease in the CTOA in the early stages of crack growth.

Since the early stages of crack growth are accompanied by a rapid decrease in CTOA, a study of the local crack tip fields in thin sheets may be useful. Hom and McMeeking [39] analyzed stationary, straight, through-thickness notches (a ratio of thickness to notch width of 5-10) using three-dimensional finite element analysis and finite deformation plasticity. Newman et al. [40] analyzed stationary, straight cracks with three-dimensional finite element analysis and small strain plasticity. Both found that substantial constraint develops in thin materials prior to crack growth, with the constraint at mid-thickness about twice the constraint that occurred at the surface ($\sigma_{yy}/\sigma_{yield} \approx 2.8$ at the mid plane).

The variation in local crack tip constraint during crack growth was studied by Sommer and Aurich [41] and Brock and Yuan [38]. For both the compact tension (CT) and middle crack tension (MT) specimens under plane strain conditions, Sommer and Aurich determined that local constraint reached and maintained a peak value near the crack tip after a small amount of crack growth; the peak value was less than predicted by HRR theory. For CT and MT specimens in plane stress, Brock and Yuan determined that the distribution in constraint ahead of the crack tip, stabilized after a small amount of crack growth. The peak constraint ($\sigma_{yy}(\theta=0°)/\sigma_{yield}$) was about 1.7 immediately ahead of the crack tip.

3

The work of Hom and McMeeking and Newman et al. indicate that thin sheet materials have substantial constraint at the mid-plane prior to crack growth. Thus, it is reasonable to expect that the through-thickness constraint variations will affect the initial stages of crack growth in thin sheets. Also, if the latter stages of crack growth approach plane stress conditions, then the work by Brock and Yuan (indicating that constraint for a growing crack stabilizes at a lower value than observed by Hom and McMeeking, and Newman et al. for stationary cracks) suggests that a single parameter may be appropriate for predicting large crack growth.

To address these issues, the enclosed work examines the stable tearing behavior of thin sheet 2024-T3 aluminum alloy. Surface CTOA values are measured by two independent methods; far-field optical microscopy and digital image correlation. Detailed metallographic evaluations of several fractured specimens were performed to quantify both the crack front shape at various stages of crack growth and the amount of slant fracture during crack growth. Measurements are made of the strain field ahead of a growing crack. The relationship between trends in CTOA, crack tunneling during crack growth, strain fields ahead of a growing crack and transition from flat-to-slant fracture is discussed.

EXPERIMENTAL PROCEDURE

Fracture tests were conducted on 2.3 mm thick (B) 2024-T3 aluminum alloy, with a yield stress and ultimate tensile stress of 360 and 495 MPa, respectively. Notched middle crack tension (MT) specimens were precracked at low and high stress levels, then fractured under displacement control. CTOA measurements were made using two different techniques.

Fracture Experiments

The MT specimen configuration is shown in Figure 1. The specimens were notched in the L-T orientation (load applied in the rolling or longitudinal direction and crack perpendicular to the rolling direction or transverse direction). Each specimen was fatigue cycled under constant amplitude loading (R = 0.02) until the total crack length was 25.4 mm (a/w = 0.33). Two different stress ranges were used: ΔS = 34.5 MPa and 172.5 MPa. The lower stress range was applied to specimens having a flat, through-thickness notch, whereas the higher stress

4

range was used for specimens having a 45° slant through-thickness notch, as shown in Figure 1. The high fatigue stress tests with the slant notches were used to minimize the "transition" effects (e.g., in the L-T orientation, an initially flat crack will "transition" into a slant crack during crack growth).

All tests were performed in displacement control and with fixed grip conditions. A total of 40 low fatigue stress MT specimens with flat initial cracks and 20 high fatigue stress MT specimens with slant initial cracks were tested. Eighteen low fatigue stress specimens and seven high fatigue stress specimens were loaded to pre-selected maximum loads, so that a limited amount of crack growth would occur. The specimens were then fatigue cycled until failure to mark the initial crack growth region. The maximum applied fatigue stress was 50-80% of the observed maximum applied stress during stable tearing and the stress ratio (R) was R=0.8. The remaining specimens were tested in displacement control until final fracture. The load and surface crack length were monitored and the surface CTOA was measured for each test.

CTOA Measurement Methods

Two independent measurement methods were used to measure CTOA during the fracture tests; Optical Microscopy (OM) and Digital Image Correlation (DIC). The OM and DIC methods were used to simultaneously measure surface CTOA on opposite sides of the specimen.

The OM setup includes (a) a long focal length microscope, (b) a video camera with resolution of 512 X 512 pixels to obtain images of the stably tearing crack, (c) a video recorder to store the images and (d) a PC with both monitor and software to precisely control the three-dimensional positioning of the long focal length microscope and also to analyze the images to obtain CTOA. The transverse magnification of the microscope was approximately 320 pixels per mm. To obtain clear images of the crack using OM, the surface of the specimen must be polished to a mirror finish and lighting of the crack region must be carefully controlled so that the crack tip region has optimum contrast and clarity. Three typical images obtained using OM are shown in Figure 2. In the first image, Figure 2a, a fatigue crack was grown about 0.75 mm under stable tearing. The second and third images, Figure 2b and 2c, contains the same crack after stable tearing of about 1.3 mm and 6 mm, respectively.

The CTOA is measured by recalling an individual image recorded on video tape and (a) locating the crack tip, (b) locating points on both crack surfaces in the range of 0.25 - 1.25 mm behind the crack tip, (c) fitting straight lines between the crack tip and each point and (d) computing the angle, θ, between the straight lines. The value of CTOA for a given crack length is defined to be the average of 3-10 sets of lines. It is important to note that OM measures CTOA in the deformed configuration, without regard for the deformations in the surrounding material.

The DIC setup includes (a) a video camera, (b) a 200 mm lens with 2X magnifier and several extension tubes, (c) translation stage for positioning of the video camera and following the growing crack, (d) video monitor to view the crack tip region, (e) video board to digitize images and (f) microcomputer with software for controlling the image acquisition process and storing images. The DIC setup is similar to previously reported systems [42-46], except that the video camera is translated parallel to the specimen surface during the experiment so that the current crack tip remains within the field of view. Note that, after each translation of the video camera, the current image and previous image overlap by at least 50 pixels so that a continuous record of crack length is maintained if the crack grows beyond the current field of view.

For the DIC, transverse magnification is approximately 125 pixels per mm. A high contrast random pattern was obtained by lightly spraying the specimen's surface with white acrylic paint and diffusely spreading black toner powder (from a laser printer) on the surface. The prepared specimen was baked at 200°F for 25 minutes to adhere the powder to the surface. A typical set of images, before and during stable crack growth, obtained by the DIC setup are shown in Figures 3a and 3b.

The DIC measurement of CTOA is somewhat more involved than that of the OM measurement procedure. Since DIC obtains the displacement vector for a small subset, the general procedure is as follows; (a) choose a particular crack tip location and deformed image, D, for analysis, (b) choose a "reference" image, R, (c) estimate the crack tip location in the deformed image, D, (d) in the region of 0.25 - 1.25 mm behind the crack tip in image D, select pairs of subsets (each pair has one subset above the crack line and one subset below the crack line) that are a distance r_i behind the crack tip, (e) compute the crack opening

6

displacement vector (u_i for upper and l_i for the lower subset) for each small subset using DIC [42-46], (f) subtract the displacement vectors for each pair of subsets, (g) estimate the normal vector for the crack line, n_i and (h) compute $CTOA_i$ for each pair of subsets using Equ. 2. The average of the $CTOA_i$ values is the estimated CTOA value. Figure 3 shows two images and two pairs of subsets that were used to define CTOA using DIC.

$$CTOA_i = 2 \tan^{-1}\left(\frac{1}{2r_i}(du_i - dl_i) \cdot n_i\right) \qquad (2)$$

Though the procedure described above is straight-forward, there are three points that must be discussed: (a) choice of "reference" image, (b) choice of subsets and (c) errors in the measurement. Relative to (a), note that the DIC method uses finite-sized subsets to estimate the displacement of the center point. If the "reference" image is an undeformed image, then the undeformed subsets will experience total strains exceeding 10% during the fracture process (most of which is plastic strain that is not recovered when the crack grows past a subset). Thus, the relative displacement used to estimate CTOA will be overestimated due to a combination of plasticity and the offset of the subset center from the crack line. To minimize this difficulty, the "reference" image is always chosen to be a deformed crack configuration that is close to the current crack length. Thus, the "reference" image already has incurred most of the intense plastic deformation that occurs during crack growth and the center point displacements should be relatively unbiased by plasticity.

Relative to (b), it is noted that subsets had to (1) be small, (2) be close to the crack line and (3) have sufficient contrast for accurate DIC analysis. Due to the random nature of the speckle pattern, it was found that there were very few pairs of useful subsets in the region 0.25 - 1.25 mm behind the crack tip. Therefore, CTOA values obtained by DIC in this work are the average of only two to four values.

Relative to (c), the primary source of error in estimating CTOA is in locating the current crack tip. The errors in locating the crack were due to lack of contrast between painted surface and crack surfaces, small crack opening near tip and a small amount of cracking of the thin paint layer near the tip. For these reasons, most of the data for CTOA was obtained by DIC using subsets more than 0.60 mm behind the crack tip.

Strain Field Measurement Method

The surface strain fields in the region immediately ahead of the crack tip were obtained using the DIC method [42-46]. Displacements were measured for 0.25 mm by 0.25 mm subsets (overlapping adjacent subsets by 0.2 mm) over a rectangular region ahead (about 0.25 mm) of the crack tip, as shown in Figure 4. A typical rectangular region was about 1.9 mm wide by about 2.6 mm high. The exact size varied since the distance between the crack tip and the edge of the current image changed during the crack growth process. The displacement data was smoothed using a two-dimensional, optimal smoothing method [47]. The smoothing program computed the estimated surface ε_{yy}, ε_{xx}, and ε_{xy} values at each displacement measurement location.

EXPERIMENTAL RESULTS

Fracture tests were conducted on 2024-T3 aluminum alloy MT specimens in the L-T orientation. Surface crack growth measurements were made using an optical microscope. Surface CTOA measurements for tearing cracks were made using the OM and DIC methods. The extent of crack tunneling during stable tearing was determined through metallographic analysis of fracture surfaces subjected to a loading history that marked the crack front. The transition from flat to slant crack growth was described by measuring the change in fracture surface height (y-direction) as a function of position through-the-thickness (z-direction) and crack length (x-direction).

Surface Crack Growth Measurements

The surface crack growth for each test was recorded as a function of the applied remote stress (S), as shown in Figure 5. Surface stable tearing was observed in the low fatigue stress (flat initial crack) tests at a stress of about 200 MPa and about 230 MPa for the high fatigue stress (slant initial crack) tests. The maximum applied stress during stable tearing was about 2% higher for the high fatigue precrack stress tests than observed in the low fatigue precrack stress tests. For crack extensions greater than twice the thickness ($\Delta a > 2B$), the stress-crack growth behavior of the two tests types were the same.

8

CTOA Measurements

The measured CTOA values as a function of crack extension for the MT specimens subjected to the low cyclic fatigue stress range are given in Figure 6. During the initial stages of surface crack growth (Δa < B) the CTOA rapidly dropped from a maximum of $12°$-$20°$ to a constant value around $6°$ for Δa > B. Excellent agreement exists between the CTOA measured by the OM and the DIC methods.

The measured CTOA values as a function of crack extension for the MT specimens subjected to the high cyclic fatigue stress are given in Figure 7. During the initial stages of surface crack growth (Δa < B) the CTOA decreased from a maximum of $6°$-$12°$ to a constant value around $6°$ for Δa < B. Again, excellent agreement exists between the CTOA measured by the OM and DIC methods. The range of initial CTOA values for the high cyclic fatigue stress tests was significantly lower than that of the low cyclic fatigue stress range tests.

Crack Tunneling Measurements

A detailed study of the crack surfaces was undertaken to improve the understanding of CTOA trends shown in Figures 6 and 7. For both low and high fatigue stress tests, a distinct change in the macroscopic appearance of the fracture surface occurs when the loading changes from fatigue cycling to stable tearing. A scanning electron microscope (SEM) photograph of a typical fracture surface from a low fatigue stress test subjected to stable tearing followed by additional fatigue cycles, is shown in Figure 8. The fracture surfaces of the high fatigue stress specimens were of similar appearance, but did not photograph well due to the $45°$ angle of crack growth.

In the SEM photograph shown in Figure 8, the stable tearing regions appear light and the fatigue regions appear dark (note that to the unaided eye, the fatigue region appears light while the stable tearing region is dark). The interface between the dark (fatigue) and light (stable tearing) region denotes the crack front profile before stable tearing. Also shown in Figure 8, a second distinct change occurs when the loading is changed from stable tearing to high-R fatigue cycling, marking the crack front profile after the stable tearing. The interfaces between the different regions were digitized for several fracture tests.

Sequences of crack front profiles from both the low and the high fatigue stress tests, with increasing amounts of stable crack extension, are shown in Figure 9. The crack fronts shown in Figure 9 represent trends in through-thickness crack extension rather than the progression of a single crack front, since each came from a different fracture test.

In the low fatigue stress tests, the cracks grew, on the average, about 0.12 mm more in the interior than on the surface during fatigue cycling, as indicated by the first profile in Figure 9a. The second crack front showed that stable tearing began in the specimen interior. This crack front revealed no surface crack extension, but the interior grew 0.5 mm. The next four crack fronts indicate that the extent of tunneling (defined as the difference between the interior crack length and the surface crack length) increased with surface crack extension. The extent of tunneling peaked at about 1.6 mm, after about 1 mm of surface crack extension and decreased for surface crack extension up to 4 mm. The extent of tunneling stabilized at about 0.4 mm for larger surface crack extensions.

The crack front profiles after fatigue cycling (the first profile in Figure 9b) at the high fatigue stress tests indicated that the crack grew, on the average, about 0.02 mm more in the interior than on the surface. An increase in the extent of tunneling to about 0.4 mm developed after small surface crack extensions and this level remained essentially constant for all larger surface crack extensions. The crack fronts profiles from the high fatigue stress tests were very similar to those from low fatigue stress tests for more than 4 mm of surface stable tearing crack growth.

The extent of tunneling that developed during stable tearing is shown in Figure 10, where the normalized extent of tunneling (the difference between the interior crack length and the surface crack length $(a_i - a_s)$ divided by the thickness (B)) is plotted as a function of the surface crack extension (Δa_s). The tunneling in the low fatigue stress tests peaked at about 70% of the thickness after about 0.8 mm of surface crack growth and dropped off to about 20% of the thickness for longer crack extensions. The extent of tunneling in the high fatigue stress tests was about 10 to 20% of the thickness for all amounts of crack extension.

10

Flat-to-Slant Transition Measurements

The measurement of the flat-to-slant transition was made for a typical MT low fatigue stress test where the specimen was fractured under displacement control. A scanning electron microscope (SEM) was used to digitize the fracture surface elevation (y) as a function of crack length (x) and through-thickness position (z). The digitized topography is shown in Figure 11 as a three-dimensional surface plot with the elevation (y-direction) of the fatigue crack region defined to be 0.0 at the end of the fatigue region. Contour lines are provided at y=-1, -0.75, -0.5, -0.25, 0, and 0.25 mm. As shown in Figure 11, the flat crack growth regime ended after about 3.6 mm of crack extension. The angle of the slant region increased from 26° just past the flat-to-slant transition (y=3.8 mm) to 40.4° after 6.4 mm of crack extension.

Strain Field Measurements

The surface crack tip strain profiles for the MT fracture tests with high and low stress fatigue cycling are given in Figures 12 and 13, respectively. The high fatigue stress level test exhibited slant crack growth for the entire fracture process. The strain profiles, obtained using a two-dimensional optimal smoothing program developed by Dohrmann and Busby [47], indicate minimal transition effects throughout the crack growth process for the high fatigue stress tests, as shown in Figure 12. A single lobe of large strain was present from the lowest loads, induced by progressive yielding along a single 45° plane through the thickness. The maximum tensile strain $(\varepsilon_{yy}|_{max} \approx 0.18)$ occurred near the crack tip for all crack growth greater than 0.10 mm.

For the low initial stress level fatigue test, the surface crack tip strains initially formed a twin lobe shape as the crack began to tunnel and simultaneously yield along two perpendicular planes through the thickness, as shown in Figure 13. As the crack grew, one lobe began to dominate, preceding the path that the crack took during the transition to 45° slant fracture. The maximum strain during the transition process was much smaller $(\varepsilon_{yy}|_{max} \approx 0.12$ for crack growth less than 2.5 mm) than for the 45° slant notch test. After transitioning to slant fracture (crack growth greater than 4.6 mm), the strain field of the low fatigue stress test had qualitatively the same shape and maximum strain as the high fatigue stress test.

DISCUSSION

The results shown in Figures 6-11 indicate that the trends in CTOA in the low and high fatigue stress tests coincide with observable changes in the fracture surfaces. The corresponding regimes of crack growth are designated; (a) initial tunneling, (b) tunneling and plane stress through-thickness yielding, and (c) fully plastic crack growth.

Initial Tunneling

As loading during the low initial fatigue stress tests is increased, crack growth initiates at the specimen mid-plane before any observable surface crack growth, as shown in Figures 9a and 10. This is consistent with the numerical work of Hom and McMeeking [39] and Newman et al. [40], both of whom showed that local crack tip constraint in thin specimens approaches plane strain conditions prior to crack growth or large scale plasticity. Thus, initial crack growth would be expected at the specimen mid-plane (crack tunneling) under locally constrained plasticity.

For the high fatigue stress tests, only slight tunneling of the crack was observed during the early stages of loading, as shown in Figures 9b and 10. Instead of significant tunneling, the high fatigue stress specimens incurred large surface strains within a narrow band of material, suggesting that plane stress through-thickness yielding was already progressing along the slant crack front.

Tunneling and Through-Thickness Yielding

Further loading increases result in surface crack growth and more tunneling in the low fatigue stress tests. The measured surface CTOA values are large (12°-20°), as shown in Figure 6, and the crack almost immediately begins to transition to a 45° slant, as shown in Figure 11. As the crack continues to grow, the extent of tunneling and the measured surface CTOA values decrease, and the area of slant crack growth increases. After about 2 thicknesses of crack growth ($\Delta a > 2B$), the transition is complete, the extent of tunneling stabilized at about 20% of the thickness, and the CTOA reached a constant value of 6°. This suggests that local constraint is decreasing as the crack grows.

The early surface crack growth in the high fatigue stress tests was not accompanied by as large of surface CTOA values as observed in the low fatigue

12

stress tests. The tunneling in the high fatigue stress tests was about 20% of the thickness for all amounts of crack extension.

It is noted that Gang et al. [48] observed similar trends in the CTOA behavior of thin sheets of 304 stainless steel. They measured large CTOA values and observed evidence of crack tunneling during the early stages of crack growth ($\Delta a<B$), and measured a constant CTOA for larger crack extensions ($\Delta a>B$). Taken together, these results indicate that the high surface CTOA values coincide with crack tunneling and through-thickness constraint. A three-dimensional, elastic-plastic finite element analysis of stationary, tunneled cracks [35] indicate that crack tunneling in thin sheets will cause higher surface crack opening displacements than observed in the interior. Thus, it is possible that the CTOA values in the interior, that may govern crack growth during the flat-to-slant transition region, are less than the measured surface values.

Fully Plastic Crack Growth

The low fatigue stress crack transitioned from flat-to-slant fracture during the initial stable crack growth ($\Delta a<2B$). Hom and McMeeking [39] showed that intense, highly localized thinning occurs just ahead of a stationary, blunted straight crack, giving rise to large shear strains along 45° planes through-the-thickness. The measured strain fields, shown in Figure 12a and 12b, indicate that large ε_{yy} strains are present in surface bands that coincide with yielding in 45° planes through-the-thickness. For longer crack lengths, the ε_{yy} strain field (Figure 12c) closely resembles the strain fields for the high fatigue stress test (Figure 13). This is consistent with a loss of through-thickness constraint for a straight crack transitioning to slant fracture. However, the continued presence of slight tunneling (about 20% of the thickness) may indicate a slight constraint effect still exists.

One should note that the relationship of the local stress and deformation fields to the fracture process is quite complex due to the highly three-dimensional nature of the slant fracture process. As noted by Zuidema and Blaauw [49], the formation of "shear lips" is a complicated phenomena, even for fatigue. Though one may use the concept of maximum shear stress to qualitatively explain the process, such an explanation cannot discern why environment, orthotropy or changes in grain structure will change the fracture from flat-to-slant.

Furthermore, it is important to realize that existing two-dimensional theories for stable crack growth assume a flat, straight, through-thickness crack front. Hence, one would expect that two-dimensional models would be unable to accurately predict the near crack tip displacement or strain behavior during the flat-to-slant transition. However, the stability of the surface CTOA values and the crack front shape during slant growth may allow two-dimensional theories to predict crack growth behavior in this regime. In this regard, it is noted that recent work by Yang et al. [50] for plane stress crack tip fields shows that the zone where several terms in the asymptotic solution are controlled by a single parameter is quite large. Hence, the use of a single parameter, such as CTOA, to characterize stable crack growth seems plausible.

For applications relative to cracks in aircraft fuselage structures, such two-dimensional models may be appropriate. Here, the prediction of residual strength is required for long cracks in thin-sheets. The cracks will have grown beyond the flat-to-slant transition and undergone substantial crack growth before failure.

SUMMARY

The stable tearing behavior of thin sheets of 2024-T3 aluminum alloy was experimentally investigated for middle crack tension specimens precracked at low (flat initial crack) and high (slant initial crack) fatigue stress, then fractured. Results of this study indicate that:

(a) The initial high surface CTOA values, when $\Delta a <$ B, coincided with the early portion of the flat-to-slant transition. The cracks were undergoing large three-dimensional crack front shape changes due to a variation in the through-thickness crack tip constraint.

(b) The flat-to-slant transition is a highly three-dimensional process. Thus, it is likely that the CTOA values in the interior, that may govern crack growth during the flat-to-slant transition region, are less than the measured surface values.

(c) The measured surface CTOA reached a constant value of 6° for $\Delta a >$ B. This coincided with the onset of 45° slant crack growth and a stabilized, slightly tunneled (about 20% of the thickness) crack front shape.

(d) After the crack transitions to the 45° slant, the crack front and local field variables are still highly three-dimensional. However, the constant CTOA values and stable crack front shape may allow the process to be approximated with two-dimensional models.

14

ACKNOWLEDGMENTS

REFERENCES

1   Kanninen, M.F., "The Analysis of Stable Crack Growth in Type 304 Stainless Steel," in Proceedings of the International Conference of Fracture, pp. 1759-1768 (1980).

2   Anderson, H., "Finite Element Representation of Stable Crack Growth," Journal of Mechanics and Physics of Solids, Vol. 21, 1973, pp. 337-356.

3   de Koning, A.U., "A Contribution to the Analysis of Quasi Static Crack Growth in Steel Materials," in Fracture 1977, Proceedings of the 4th International Conference on Fracture, Vol. 3, pp. 25-31.

4   Wells, A.A., "Unstable Crack Propagation in Metals: Cleavage and Fast Fracture," in Proceedings of the Cranfield Crack Propagation Symposium, Vol. 1, 1961, pp. 210-230.

5   Wells, A.A., "Application of Fracture Mechanics at and Beyond General Yielding," British Welding Journal, Vol. 11, 1961, pp. 563-570.

6   Wells, A.A., "Notched Bar Tests, Fracture Mechanics and Brittle Strengths of Welded Structures," British Welding Journal, Vol. 12, 1963, pp. 2-13.

7   Broberg, K.B., "On stable crack growth," Journal of the Mechanics and Physics of Solids, Vol. 23, 1975, pp. 215-237.

8   Orowan, E., "Fracture and Strength of Solids," Report of Progress in Physics, Physical Society of London, Vol. 12, pp. 185-233, 1949.

9   Rice, J.R., "A Path Independent Integral and the Approximate Analysis of Strain Concentration by Notches and Cracks," ASME Journal of Applied Mechanics, Vol. 35, 1968, pp. 379-368.

10   Landes, J.D., and Begley, J.A., "The Effect of Specimen Geometry on J_{Ic}," ASTM STP 514, Part II, 1972, pp. 24-39.

11   Hutchinson, J.W., "Plastic Stress and Strain Fields at a Crack Tip," J. Mech. Phys. of Solids, Vol. 16, 1968, pp. 13-31.

12   Rice, J.R. and Rosengren, G.F., "Plane Strain Deformation Near a Crack Tip in a Power-Hardining Material," _J. Mech. Phys. of Solids_, Vol. 16, 1968, pp. 1-12.

13   Dean, R.H., "Elastic-Plastic Steady Crack Growth in Plane Stress", _ASTM STP 803_, ASTM Philadelphia, 1983, pp. 83.

14   Shih, C.F., de Lorenzi, H.G. and Andrews W.R., "Studies on Crack Initiation and Stable Crack Growth", _ASTM STP 668_, ASTM, Philadelphia, 1979, pp. 65-120.

15   Shih, C.F., Dean, R.H., and German M.D., "On J-Controlled Crack Growth: Evidence, Requirements and Applications General Electric Co. T13 Report Schenectady, New York, 1981.

16   Hutchinson, J.W., and Paris, P.C., "Stability Analysis of J-Controlled Crack Growth," _ASTM STP 668_, ASTM, Philadelphia, 1979, pp. 37-64.

17   McMeeking, R.M., and Parks, D.M., "On Criteria for J-Dominance of Crack-Tip Fields in Large-Scale Yielding", _ASTM STP 668_, ASTM, Philadelphia, 1979, pp. 175-194.

18   Kang, B.S.-J. and Kobayashi, A.S., "J-Estimation Procedure based on Moiré interferometry data," _ASME Journal for Pressure Vessel Technology_, Vol. 110, pp. 291-300, 1988.

19   Kang, B.S.-J. and Kobayashi, A.S., "Stable Crack Growth in Aluminum Tensile Specimens," _Experimental Mechanics_, Vol. 27, pp. 234-245, 1987.

20   Dadkhah, M.S. and Kobayashi, A.S., "HRR Field of a Moving Crack, an Experimental Analysis," _Engineering Fracture Mechanics_, Vol. 34, pp. 253-262, 1989.

21   Dadkhah, M.S. and Kobayashi, A.S., "Further Studies in the HRR Field of a Moving Crack, an Experimental Analysis," _Journal of Plasticity_, Vol. 6, pp. 635-650, 1990.

22   Kobayashi, A.S., Dadkhah, M.S. and Kang, B.S.-J. "J-Integral and HRR Field of a Stably Growing Crack, an Experimental Analysis," UWA/DME/TR-90/65, Office of Naval Research, April 1990.

23   Drinnon, R.H. and Kobayashi, A.S., "J-Integral and HRR Field Associated with Large Crack Extension," _Engineering Fracture Mechanics_, Vol. 41, No. 5, pp. 684-694, 1992.

24   Dadkhah, M.S., Kobayashi, A.S., and Morris, W.L., "Crack Tip Displacement Fields and J_r-Curves for Four Aluminum Alloys," _ASTM STP 1131_, Vol. II, pp. 135-153, 1992.

25   Davidson, D.C., "The Distribution of Strain with Crack Tip Plastic Zones," _Engineering Fracture Mechanics_, Vol. 25, No. 1, pp. 123-132, 1986.

26   Rice, J.R., and Sorensen, E.P., "Continuing Crack-Tip Deformation and Fracture for Plane strain Crack Growth in Elastic-Plastic Solids," Journal of Mechanics and Physics of Solids, Vol. 26, 1978, pp. 163-186.

27   Shih, C.F.," Studies on Crack Initiation and Stable Crack Growth," ASTM STP. 668, 1979, pp. 65-120.

28   Shih, C.F., de Lorenzi, H.G. and Andrews W.R., "Elastic-Plastic Fracture", ASTM STP 668, ASTM, Philadelphia, 1979, pp. 65.

29   Hellman, D. and Schwalbe, K.-H., "Geometry and Size Effects on J-R and δ-R Curves Under Plane Stress Conditions," ASTM STP 833, pp. 577-605, 1984.

30   Hellman, D. and Schwalbe, K.-H., "On the Experimental Determination of CTOD Based R-Curves," Proceedings of the Conference on Crack Tip Opening Displacement in Elastic-Plastic Fracture Mechanics, Springler-Verlag, pp. 115-132, 1986.

31   Kanninen, M.F., "The Analysis of Stable Crack Growth in Type 304 Stainless Steel," in Proceedings of the International Conference of Fracture 1980, pp. 1759-1768.

32   Kanninen, M.F., Popelar, C.H., and Broek, D. "A Critical Survey on the Application of Plastic Fracture Mechanics to Nuclear Pressure Vessels and Piping," Nuclear Engineering and Design, 1981, Vol., 67, pp. 27-55.

33   Kanninen, M.F., Advanced Fracture Mechanics, Oxford University Press, 1985.

34   Demofonti, G. and Rizzi, L., "Experimental Evaluation of CTOA in Controlling Unstable Ductile Fracture Propagation," ESIS Pub. 9, 1991, pp. 693-703.

35   Newman, J.C., Jr., Dawicke, D.S., and Bigelow, C.A., "Finite-Element Analysis and Measurement of CTOA During Stable Tearing in a Thin-Sheet Aluminum Alloy," Proceedings from the International Workshop on Structural Integrity of Aging Airplanes, April 1992.

36   Newman, J.C., Jr. "An Elastic-Plastic Finite Element Analysis of Crack Initiation, Stable Crack Growth, and Instability," ASTM STP 833, 1984, pp. 93-117.

37   Newman, J.C., Jr., Shivakumar, K.N., and McCabe, D.E., "Finite Element Fracture Simulation of A533B Steel Sheet Specimens", ESIS Pub. 9, 1991, pp. 117-126.

38   Brocks, W. and Yuan, H. "Numerical Studies on Stable Crack Growth", ESIS Pub. 9, 1991, pp. 19-33.

39   Hom, C.L. and McMeeking, R.M., "Large Crack Tip Opening in Thin, Elastic-Plastic Sheets," International Journal of Fracture, Vol. 45, pp. 103-122, 1980.

40   Newman, J.C., Jr., Bigelow, C.A., and Shivakumar, K.N., "Three-Dimensional Elastic-Plastic Finite-Element Analysis of Constraint Variations in Cracked Bodies," NASA TM 107704, 1993.

41   Sommer, E. and Aurich, D., "On the Effect of Constraint on Ductile Fracture," Proceedings of the European Symposium on Elastic-Plastic Fracture Mechanics, ESIS/EGF Publication 9, pp. 141-175, 1991.

42   Sutton, M.A., Bruck, H.A., Chae, T.L., and Turner, J.L., "Experimental Investigations of Three-Dimensional Effects Near a Crack Tip Using Computer Vision," International Journal of Fracture, Vol. 53, 1991, pp. 201-228.

43   Sutton, M.A., Bruck, H.A., and McNeill, S.R., "Determination of Deformations Using Digital Correlation with the Newton Raphson Method for Partial Differential Correction," Experimental Mechanics, Vol. 29 (3), 1989, pp. 261-267.

44   Sutton, M.A., Turner, J.L., Chae, T.L., and Bruck, H.A., "Development of a Computer Vision Methodology for the Analysis of Surface Deformation in Magnified Image," ASTM STP 1094, MICOM 90. 1990, pp. 109-132.

45   Sutton, M.A., Turner, J.L., Bruck, H.A., and Chae, T.L., "Full-Field Representation of the Discretely Sampled Surface Deformation for Displacement and Strain Analysis," Experimental Mechanics, Vol. 31 (2), 1991, pp. 168-177.

46   Sutton, M.A. and McNeill, S.R., "The Effects of Subpixel Image Restoration on Digital Correlation Error Estimates," Optical Engineering, Vol. 27 (3), 1988, pp. 163-175.

47   Dohrmann, C.R. and Bushy, H.R., "Spline Function Smoothing and Differentiation of Noisy Data on a Rectangular Grid," Proceedings of the VI International Conference on Experimental Mechanics, pp. 843-849, 1988.

48   Gang, H., Sutton, M.A., Chao, Y.J. and Lyons, J.S., "Ductile Crack Blunting, Initiation and Crack Growth Analysis of 304 Stainless Steel Specimens by Computer Vision," Proc. of Spring SEM Conference, 1993.

49   Zuidema, J. and Blaauw, H.S., "Slant Fatigue Crack Growth in Al 2024 Sheet Material," Engineering Fracture Mechanics, Vol. 29, No. 4, pp 401-413, 1988.

50   Yang, S., Chao, Y.J. and Sutton, M.A., "Complete Theoretical Analysis for Higher Order Asymptotic Terms and the HRR Zone at a Crack Tip for Mode I and Mode II Loading of a Hardening Material," ACTA Mechanica, Vol. 98, pp. 79-98, 1993.
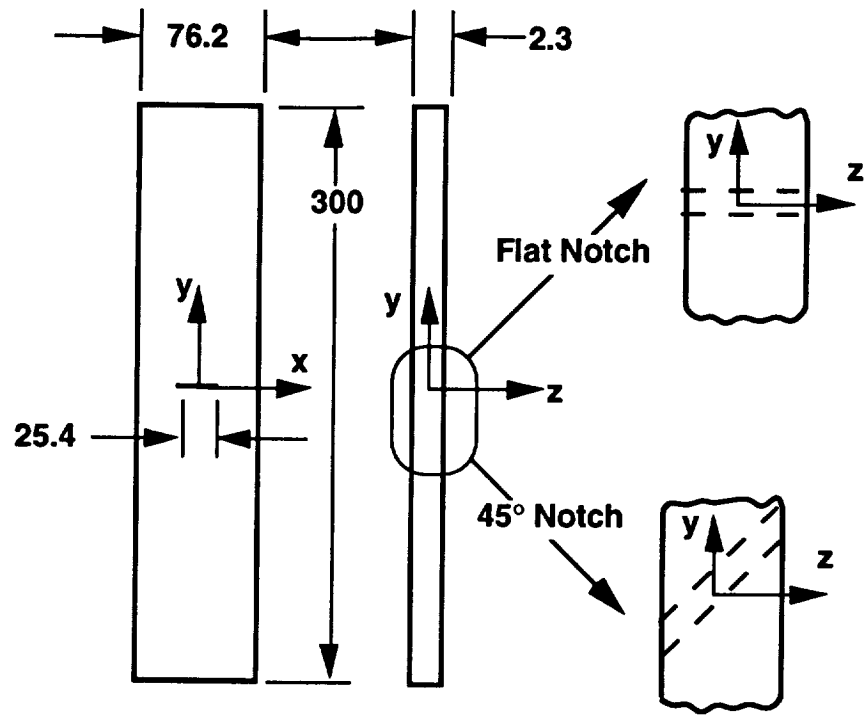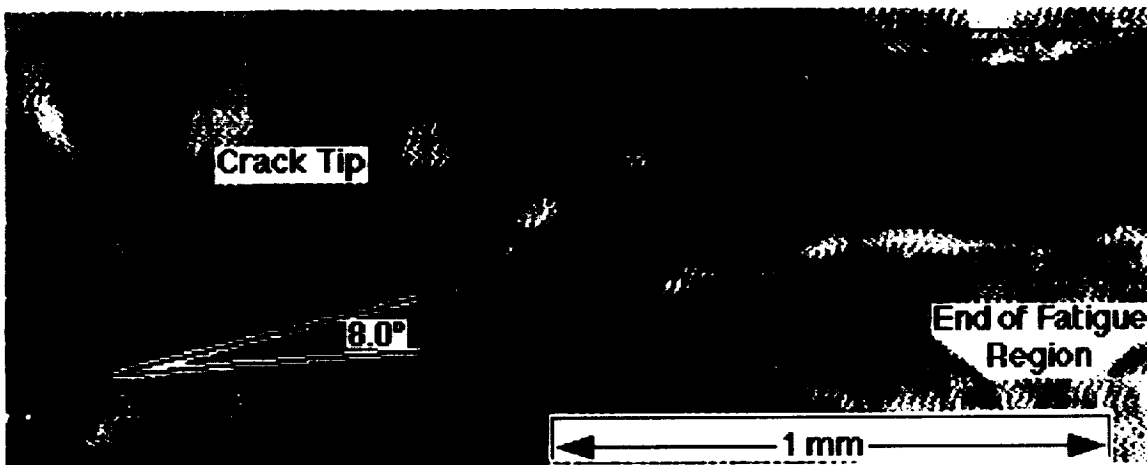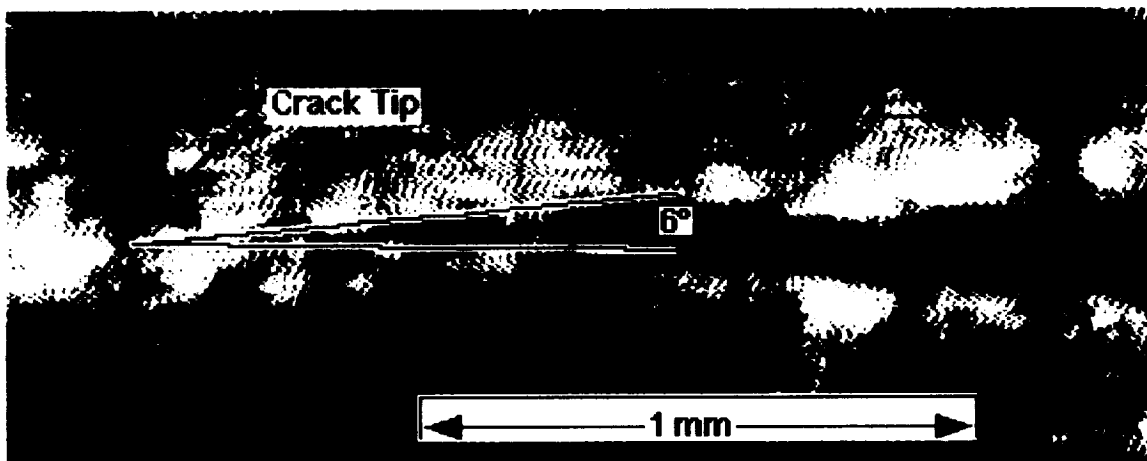
Note: All dimensions in mm

Figure 1   Schematic of flat notch and 45° notch MT specimens.
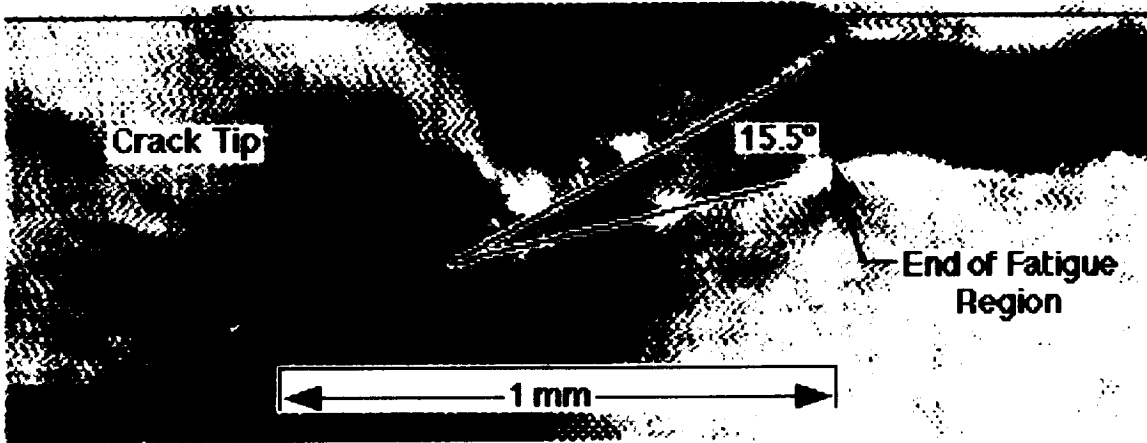
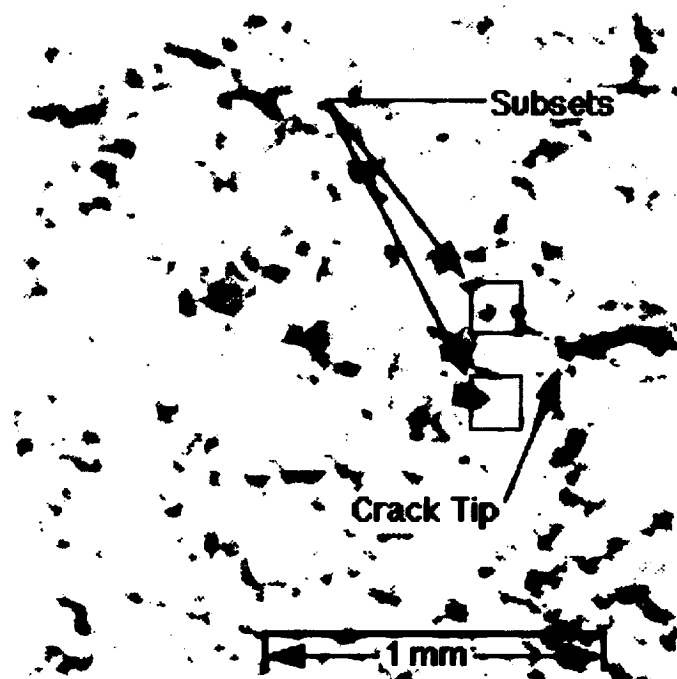a.   OM image after about 0.75 mm of stable tearing

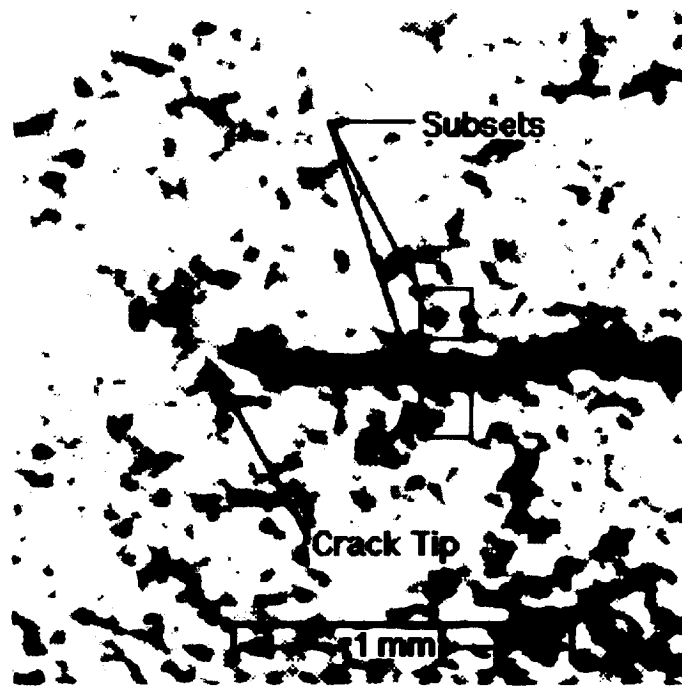b.   OM image after about 1.3 mm of stable tearing

c.   OM image after about 6 mm of stable tearing

Figure 2   Typical OM images and CTOA measurements for stable tearing cracks in 2.3 mm thick 2024-T3 aluminum alloy.
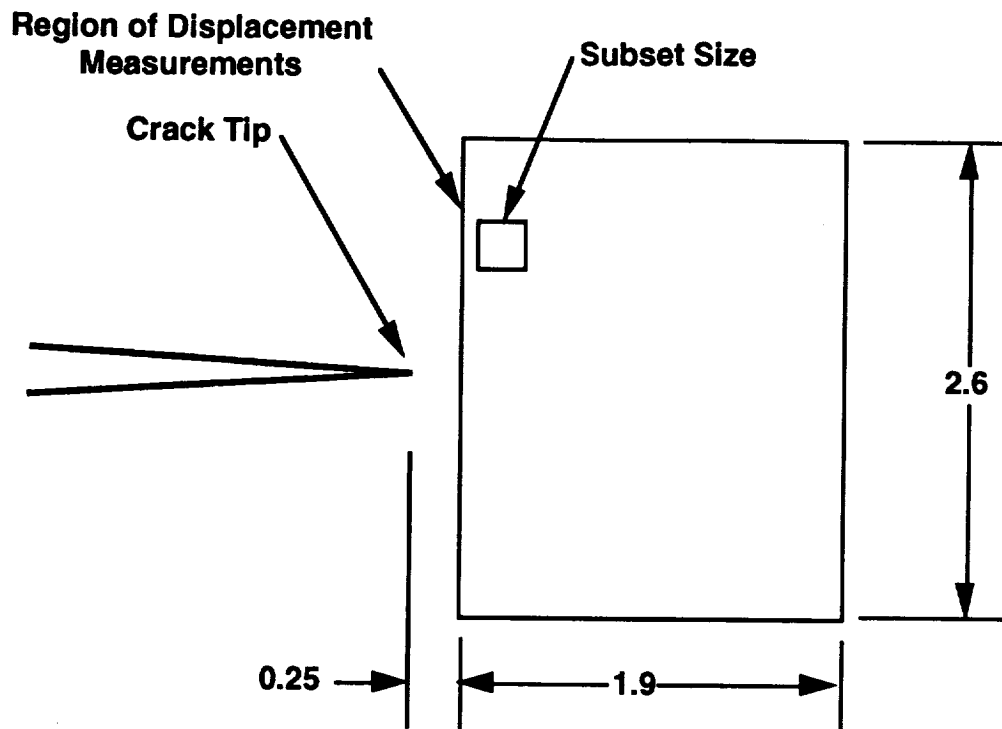
a. Before crack extension

b. During crack extension

Figure 3   Images of a stably tearing crack obtained from the DIC method and the subsets used to obtain the CTOA.

Note: all dimensions in mm

Figure 4.   Location of the region and the subset size used to calculate the strain field behavior for a stably tearing crack.
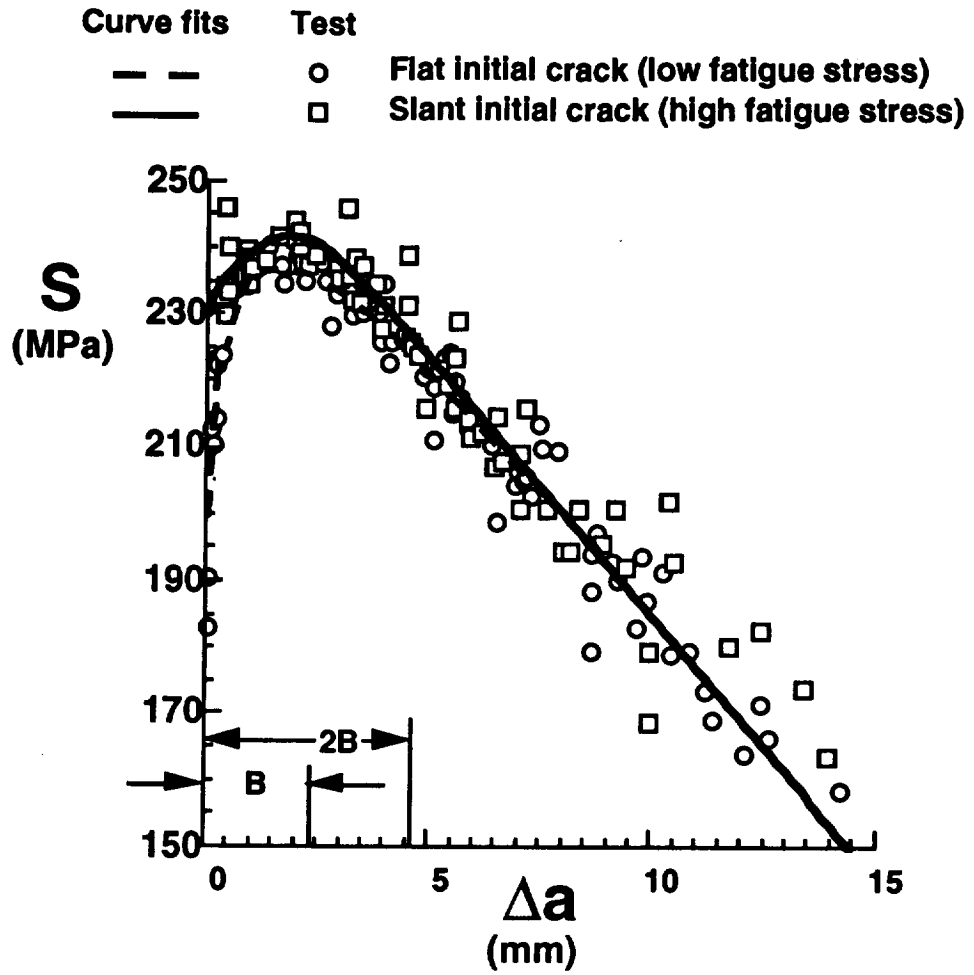
Figure 5.   Crack growth behavior of the low fatigue stress and high fatigue stress fracture tests.
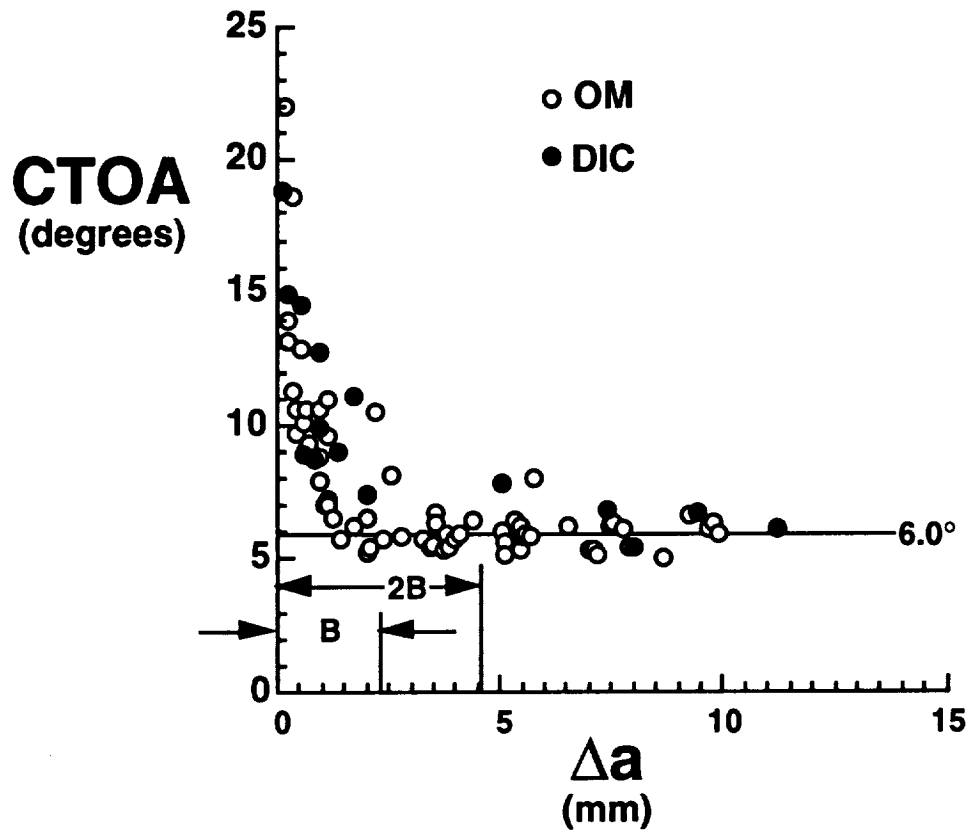
Figure 6.   Crack tip opening angles measured using the optical microscopy and digital image correlation methods for the 76.2 mm wide, 2.3 mm thick MT specimens for low fatigue stress tests.
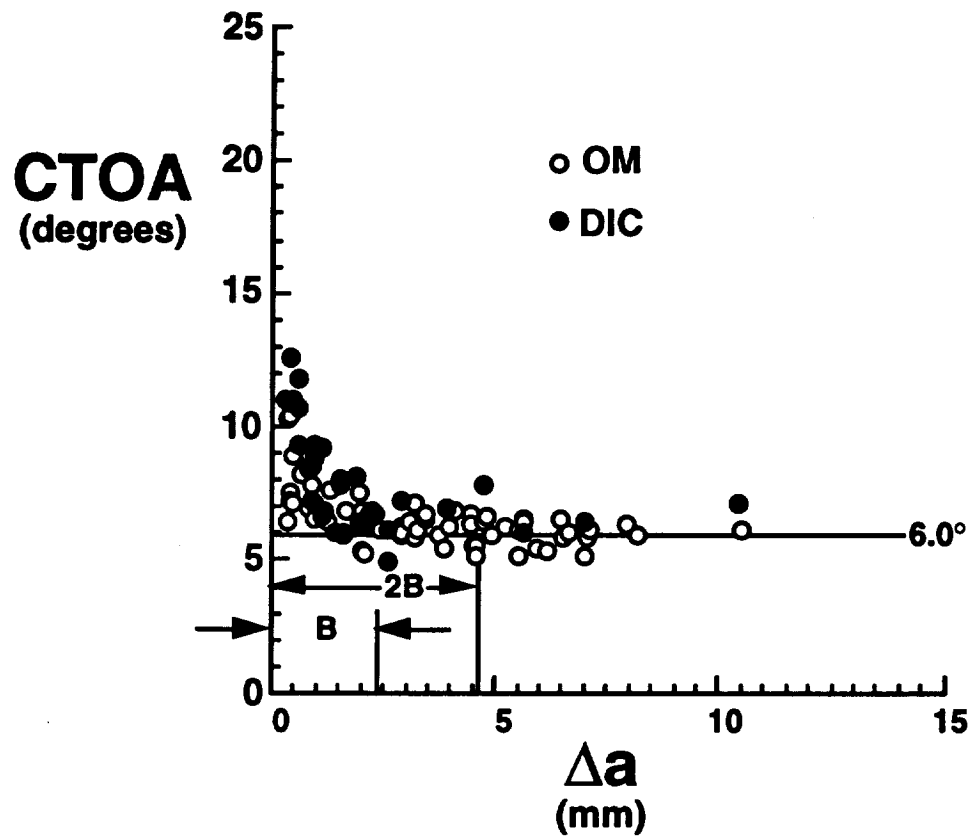
Figure 7.   Crack tip opening angles measured using the optical microscopy and digital image correlation methods for the 76.2 mm wide, 2.3 mm thick MT specimens for high fatigue stress tests.

(0.079 in.)
0.2 mm

(0.079 in.)
0.2 mm

(0.039 in.)
1 mm
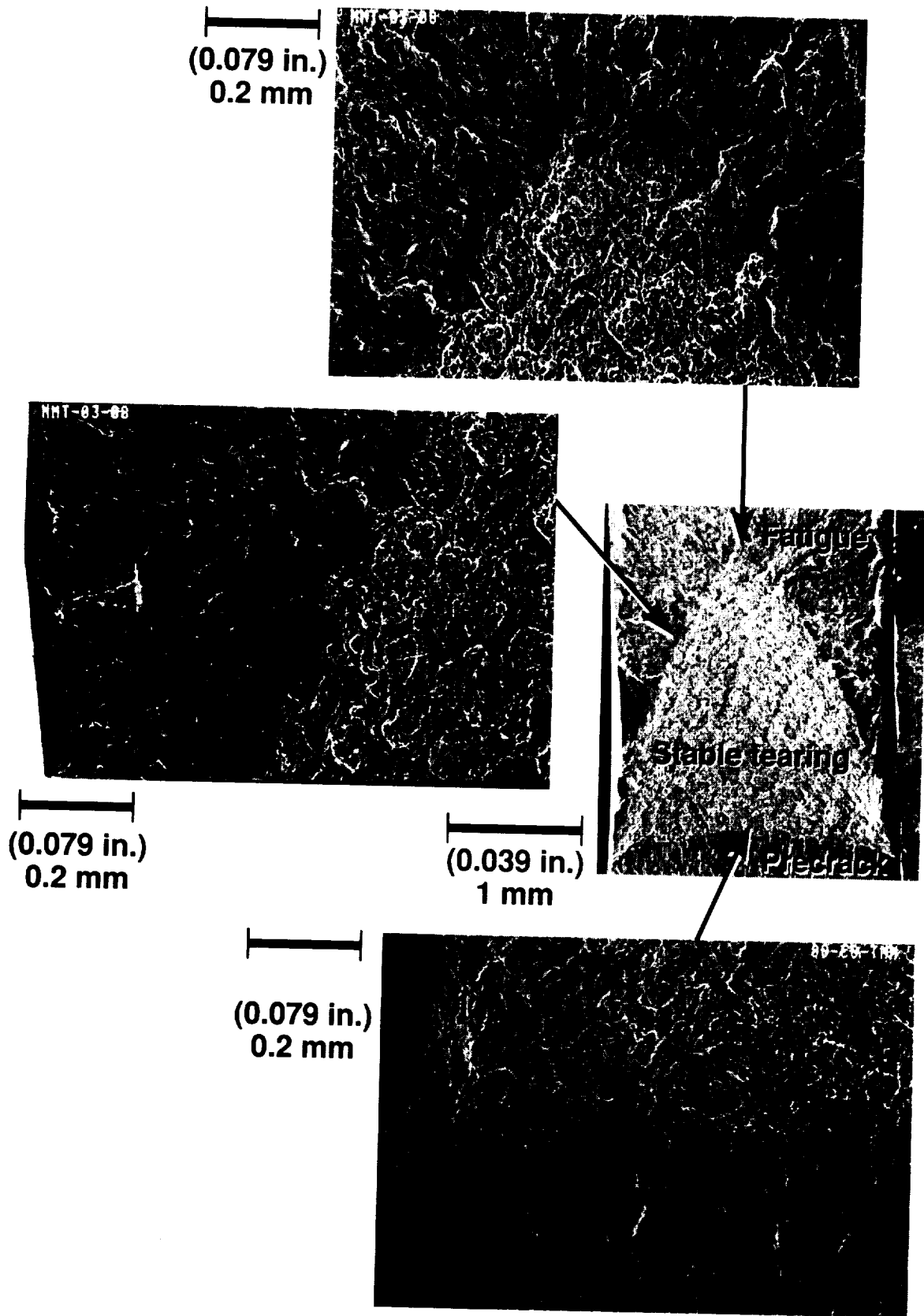
(0.079 in.)
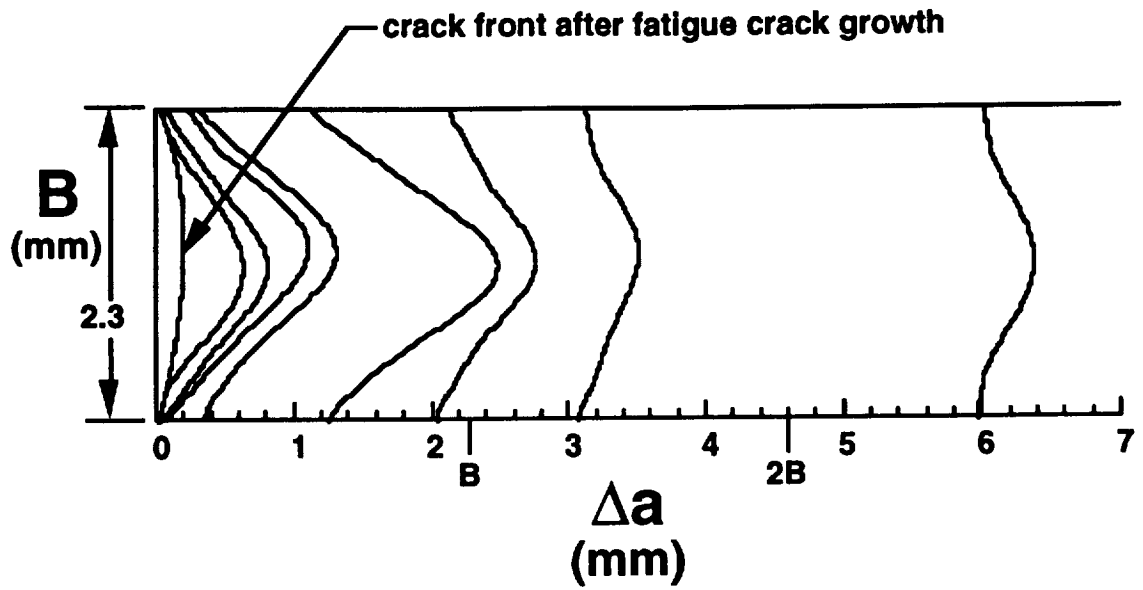0.2 mm

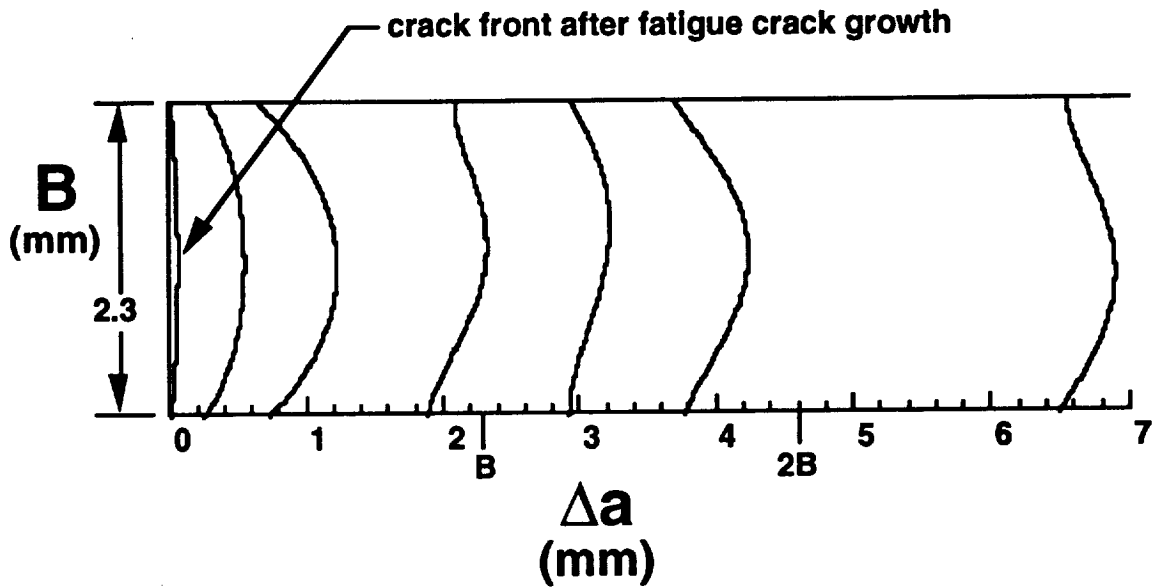Fatigue

Stable tearing

Precrack

Figure 8.   Scanning electron microscope photographs of the fracture surface of a 76.2 mm wide, 2.3 mm thick MT specimen with a low fatigue stress, subjected to stable tearing followed by high-R fatigue cycling.

26

crack front after fatigue crack growth

B (mm)

2.3

0   1   2 B   3   4   2B   5   6   7

Δa
(mm)

a.   Low fatigue stress tests, ΔS = 34.5 MPa

crack front after fatigue crack growth

B (mm)

2.3

0   1   2 B   3   4   2B   5   6   7

Δa
(mm)

b.   High fatigue stress tests, ΔS = 172.5 MPa

Figure 9.   Crack front profiles after stable tearing for MT specimens, low and high fatigue stress fracture tests.
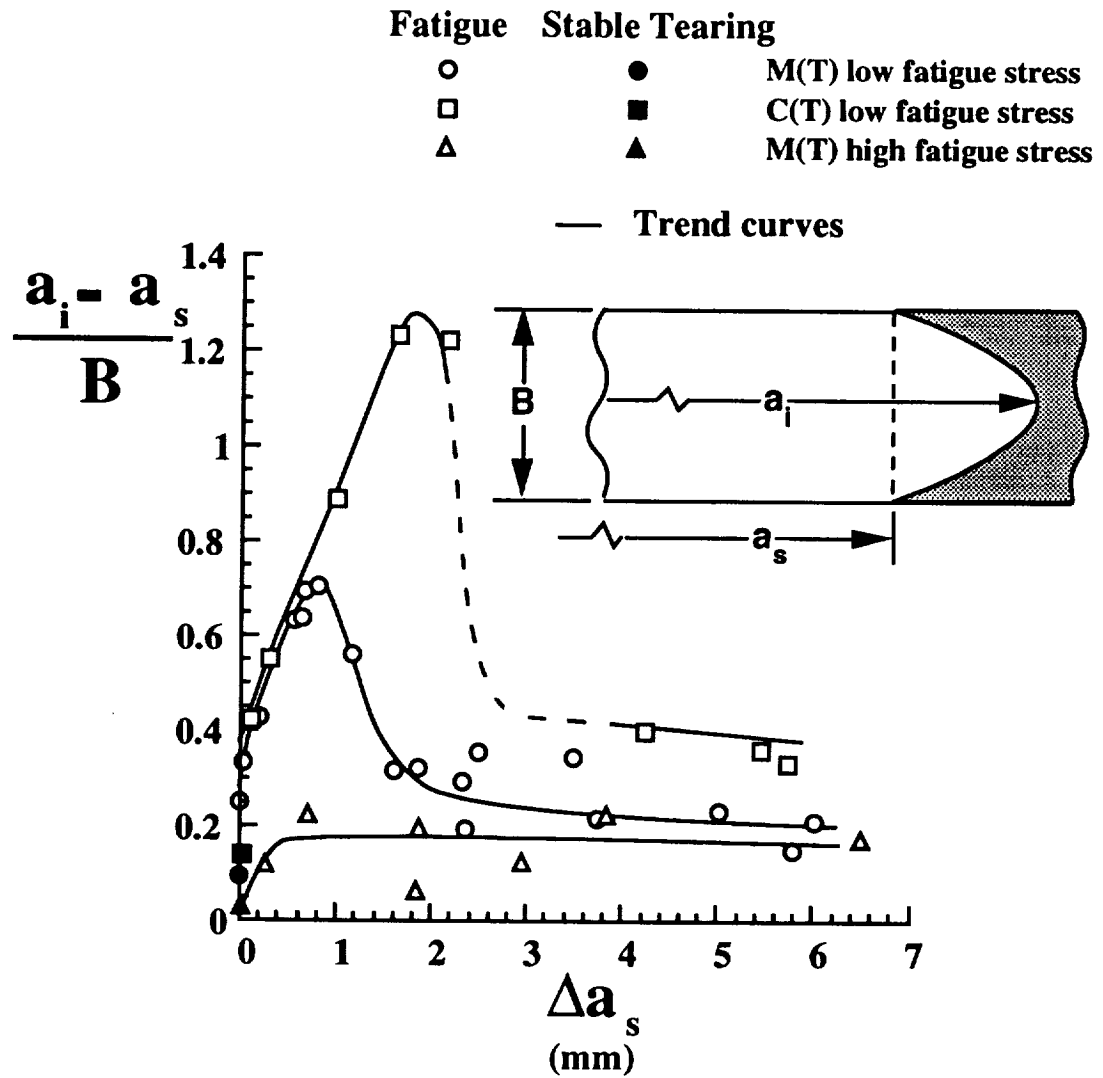
Figure 10. The extent of crack tunneling for the 76.2 mm wide, 2.3 mm thick MT specimen fracture tests.
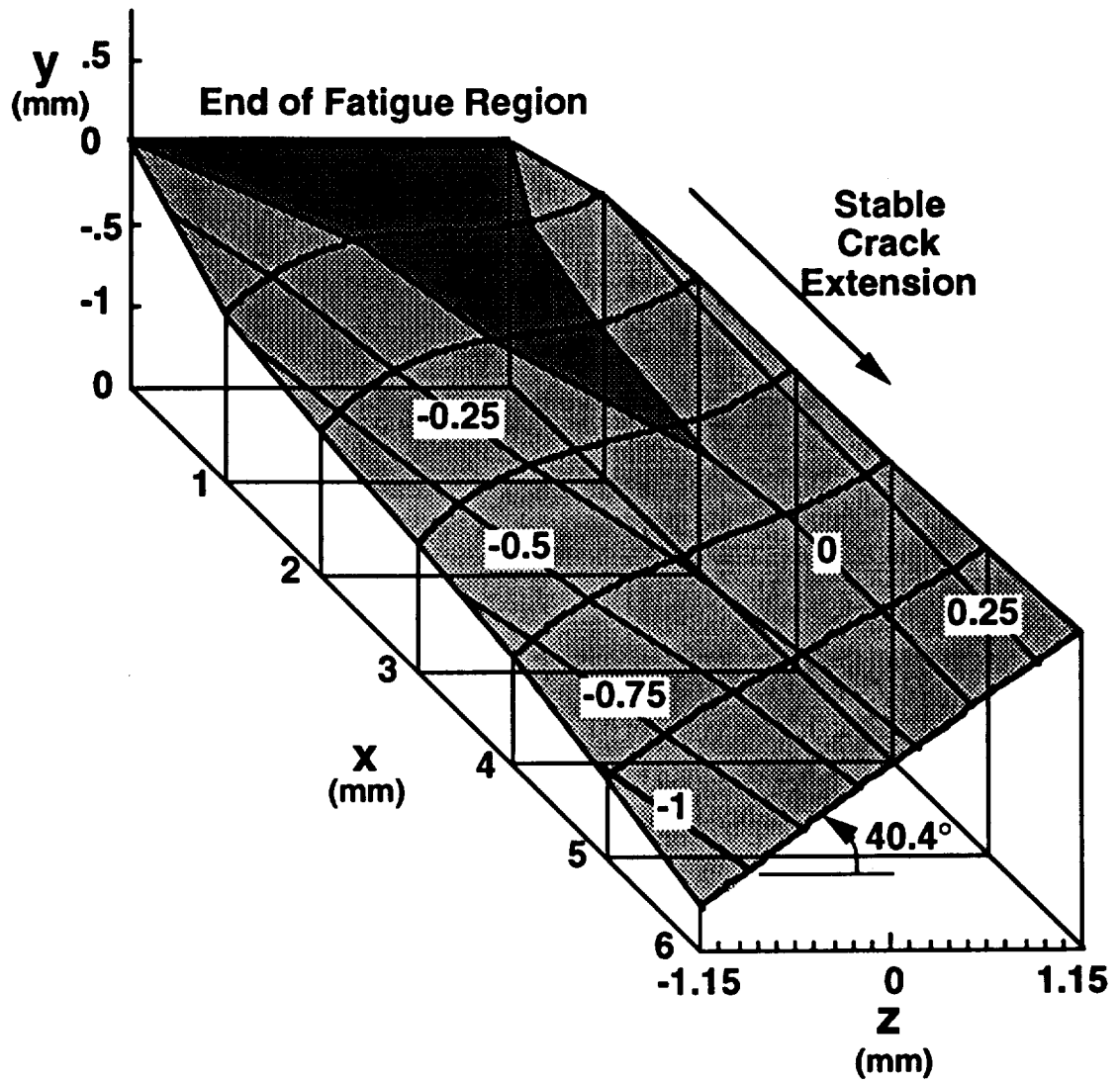
Figure 11. The fracture surface topology for a 76.2 mm wide, 2.3 mm thick MT specimen (low fatigue stress, ΔS = 34.5 MPa) fracture test.
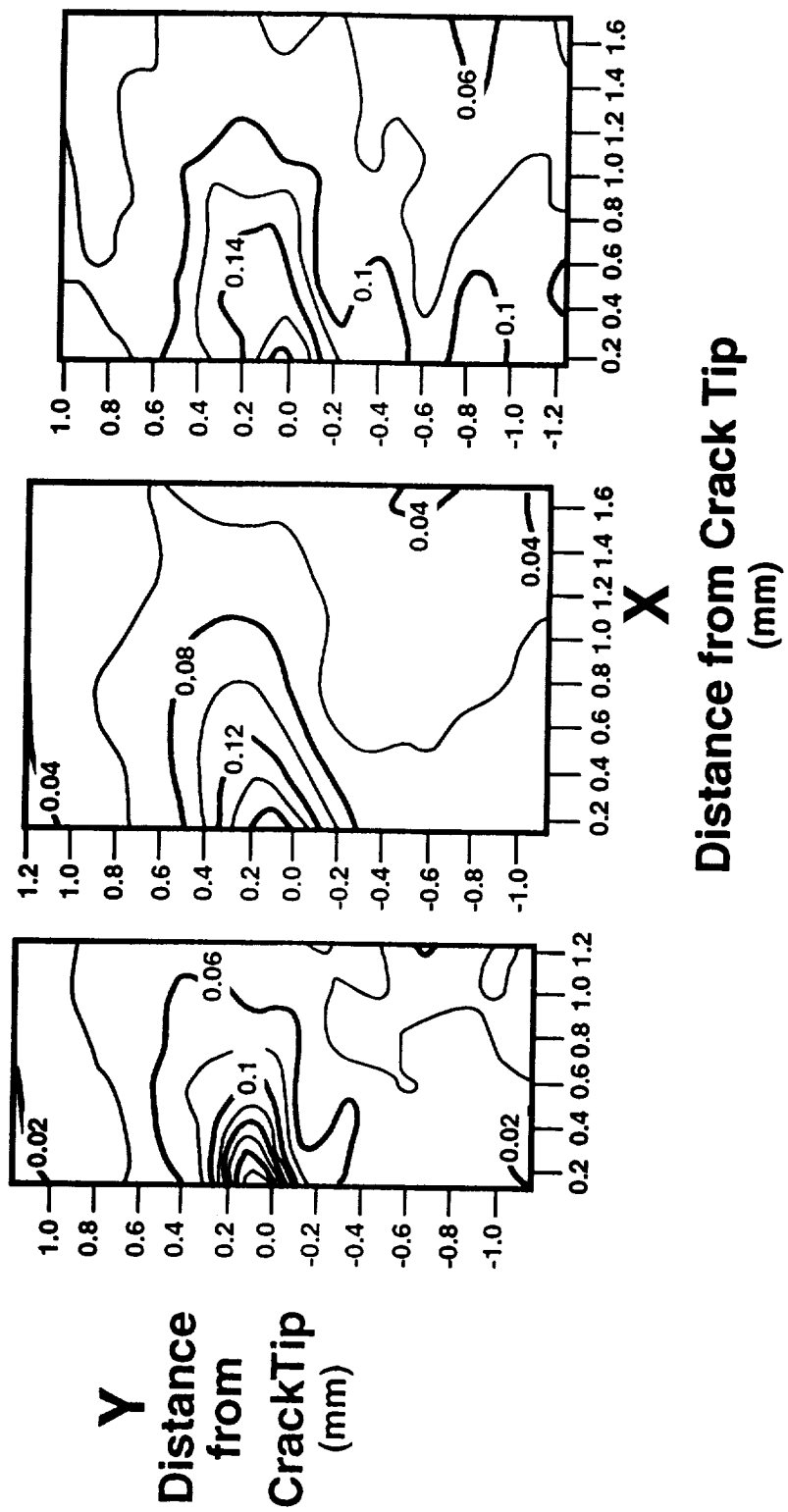
Y
Distance
from
CrackTip
(mm)

X

Distance from Crack Tip
(mm)

a. Δa = 0.60 mm   b. Δa = 2.0 mm   c. Δa = 9.0 mm

Figure 12.   ε$_{yy}$ strain fields for a high stress range (172.5 MPa, 45° initial notch) fatigue cycling fracture test.

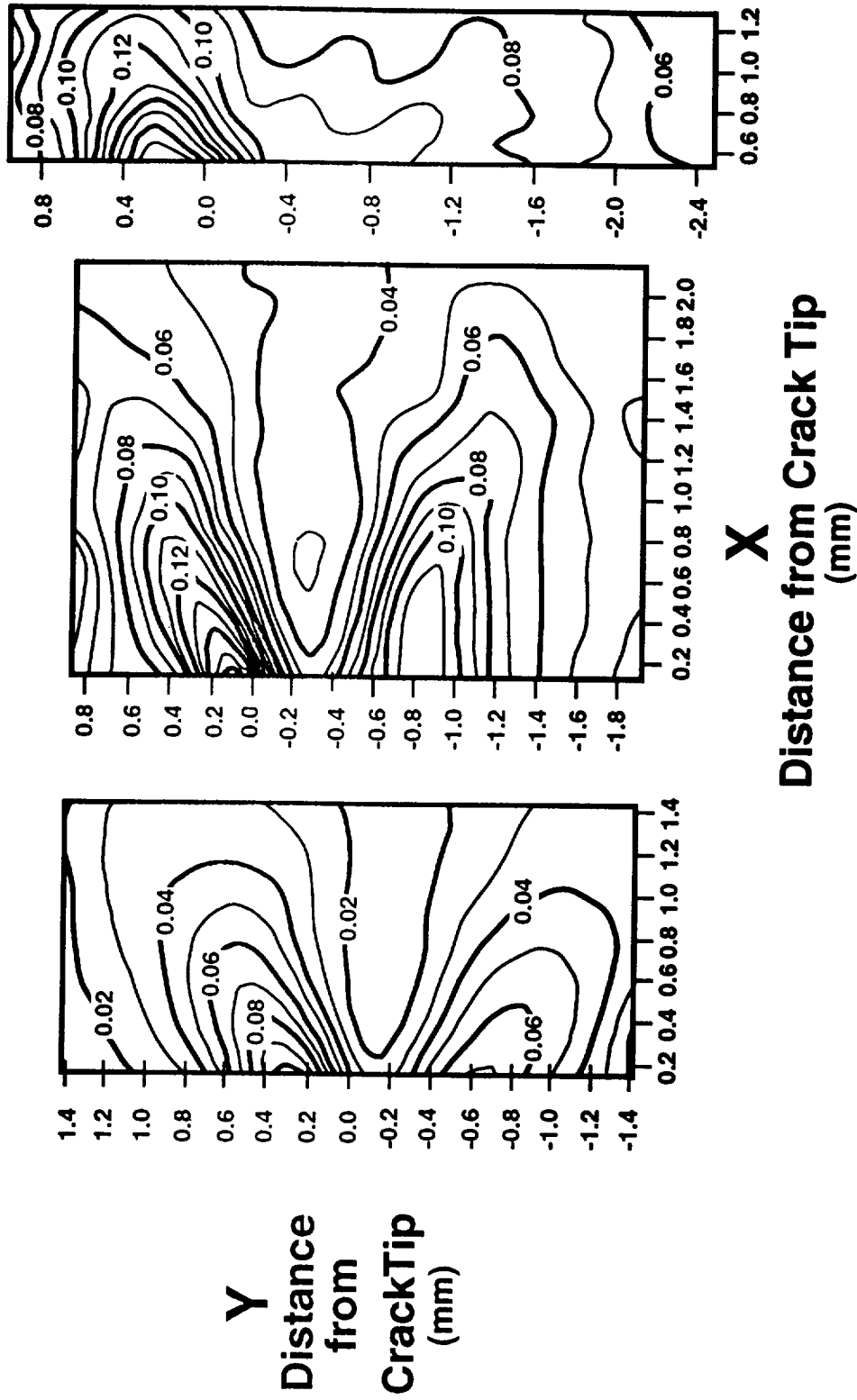Figure 13. ε_{yy} strain fields for a low stress range (34.5 MPa) fatigue cycling fracture test.

a. Δa = 0.80 mm   b. Δa = 2.55 mm   c. Δa = 12.8 mm

REPORT DOCUMENTATION PAGE

Public reporting burden for this collection of information is estimated to average 1 hour per response, including the time for reviewing instructions, searching existing data sources, gathering and maintaining the data needed, and completing and reviewing the collection of information. Send comments regarding this burden estimate or any other aspect of this collection of information, including suggestions for reducing this burden, to Washington Headquarters Services, Directorate for Information Operations and Reports, 1215 Jefferson Davis Highway, Suite 1204, Arlington, VA 22202-4302, and to the Office of Management and Budget, Paperwork Reduction Project (0704-0188), Washington, DC 20503.

1. AGENCY USE ONLY (Leave blank)	2. REPORT DATE September 1993	3. REPORT TYPE AND DATES COVERED Contractor Report

4. TITLE AND SUBTITLE

Crack-Tip-Opening Angle Measurements and Crack Tunneling Under Stable Tearing In Thin Sheet 2024-T3 Aluminum Alloy

5. FUNDING NUMBERS

NAS1-19399

NAG1-148

6. AUTHOR(S)

D. S. Dawicke and M. A. Sutton

WU 538-02-10-01

7. PERFORMING ORGANIZATION NAME(S) AND ADDRESS(ES)

Analytical Services and Materials Inc.
Hampton, VA 23666

University of South Carolina
Columbia, SC 29208

8. PERFORMING ORGANIZATION REPORT NUMBER

9. SPONSORING / MONITORING AGENCY NAME(S) AND ADDRESS(ES)

National Aeronautics and Space Administration
Langley Research Center
Hampton, VA 23681-0001

10. SPONSORING / MONITORING AGENCY REPORT NUMBER

NASA CR-191523

11. SUPPLEMENTARY NOTES
Langley Technical Monitor: Dr. C. E. Harris
Final Report

12a. DISTRIBUTION / AVAILABILITY STATEMENT

Unclassified - Unlimited

Subject Category 24

12b. DISTRIBUTION CODE

13. ABSTRACT (Maximum 200 words)

The stable tearing behavior of thin sheets 2024-T3 aluminum alloy was studied for middle crack tension specimens having initial cracks that were: (a) flat cracks (low fatigue stress) and (b) 45° through-thickness slant cracks (high fatigue stress). The critical CTOA values during stable tearing were measured by two independent methods, optical microscopy and digital image correlation. Results from the two methods agreed well.

The CTOA measurements and observations of the fracture surfaces have shown that the initial stable tearing behavior of low and high fatigue stress tests is significantly different. The cracks in the low fatigue stress tests underwent a transition from flat-to-slant crack growth, during which the CTOA values were high and significant crack tunneling occurred. After crack growth equal to about the thickness, CTOA reached a constant value of 6° and after crack growth equal to about twice the thickness, crack tunneling stabilized. The initial high CTOA values, in the low fatigue crack tests, coincided with large three-dimensional crack front shape changes due to a variation in the through-thickness crack tip constraint. The cracks in the high fatigue stress tests reach the same constant CTOA value after crack growth equal to about the thickness, but produced only a slightly higher CTOA values during initial crack growth. For crack growth on the 45° slant, the crack front and local field variables are still highly three-dimensional. However, the constant CTOA values and stable crack front shape may allow the process to be approximated with two-dimensional models.

14. SUBJECT TERMS
Cracks; Fracture; Crack-tip-opening angle; Crack tunneling; 2024-T3 aluminum alloy; Strain fields

15. NUMBER OF PAGES
32

16. PRICE CODE
A03

17. SECURITY CLASSIFICATION OF REPORT Unclassified	18. SECURITY CLASSIFICATION OF THIS PAGE Unclassified	19. SECURITY CLASSIFICATION OF ABSTRACT	20. LIMITATION OF ABSTRACT